

Successive Eigenvalue Removal for Multi-Soliton Spectral Amplitude Estimation

Alexander Span, Vahid Aref, Henning Bülow, and Stephan ten Brink

Abstract—Optical nonlinear Fourier transform-based communication systems require an accurate estimation of a signal’s nonlinear spectrum, computed usually by piecewise approximation methods on the signal samples. We propose an algorithm, named successive eigenvalue removal, to improve the spectrum estimation of a multi-soliton pulse. It exploits a property of the Darboux transform that allows removing eigenvalues from the nonlinear spectrum. This results in a smaller pulse duration and smaller bandwidth. The spectral coefficients are estimated successively after removing the eigenvalues of a signal. As a beneficial application, we show that the algorithm decreases the computational complexity by iteratively reducing the pulse duration.

Index Terms—Nonlinear Optical Fiber Communications, Nonlinear Fourier Transform, Nonlinear Frequency Division Multiplexing, Multi-soliton

I. INTRODUCTION

For the nonlinear optical fiber channel, modeled by the nonlinear Schrödinger equation (NLSE), the nonlinear Fourier transform (NFT) maps a pulse from time domain into a so-called nonlinear Fourier domain where the signal transformation along the link can be described by simple equations [1]. This motivates the modulation of data in the nonlinear spectrum, which needs the computation of the inverse NFT and NFT at the transmitter and receiver, respectively. A special class of transmission pulses, considered here, are multi-solitons which are characterized in the nonlinear spectrum simply by some pairs of eigenvalue and corresponding spectral amplitude.

The Darboux transform (DT) [2] is a common inverse NFT algorithm to generate multi-soliton signals iteratively. Although this inverse NFT is rather simple with low complexity, the forward NFT is a more challenging task in order to compute the eigenvalues and their spectral amplitudes. Various numerical methods have been developed so far to compute the spectral amplitudes, see [1], [3]–[7]. These algorithms are mainly based on numerically solving the Zakharov-Shabat system (ZSS) by a piecewise approximation method. The approximation error is rectified usually by a rather large number of signal samples or by using higher-order approximation methods [6], [7]. Besides, the forward-backward (FB) method (called bi-directional method in [4]) further reduces the numerical errors of all one-step discretization NFT methods [3].

Date of current version April 7, 2022.

A. Span and S. ten Brink are with Institute of Telecommunications, University of Stuttgart, Stuttgart, Germany (E-mail: {alexander.span,tenbrink}@inue.uni-stuttgart.de).

V. Aref and H. Bülow are with Nokia Bell Labs, Stuttgart 70435, Germany (E-mail: {vahid.aref,henning.buelow}@nokia-bell-labs.com).

The accuracy of this method is recently improved by some modification in [8].

Here, we propose a new approach for the forward NFT based on the Darboux transformation. Although the DT is commonly known for adding eigenvalues, it is also able to remove eigenvalues from a given solitonic pulse [9]. Applying the DT carefully removes an eigenvalue from the pulse’s nonlinear spectrum with a simple change on the remaining nonlinear spectrum of the pulse. As we explain in Sec. II, $a(\lambda)$ will be changed but the b —values remain the same. While this property of the DT is known for a long time, it has not yet been used for the detection of the nonlinear spectrum.

We propose the Successive Eigenvalue Removal (SER) algorithm where the spectral coefficients are estimated one by one successively. Following a predefined order, an eigenvalue and its spectral coefficient are estimated and then removed from the nonlinear spectrum. This process is repeated on the remaining pulse until all eigenvalues are removed. This algorithm is beneficial as removing an eigenvalue can reduce the pulse duration as well as the bandwidth (smoother variations). Both reductions can decrease the number of numerically required pulse samples and thus decrease the total computational complexity of the NFT computation. We discuss that the SER algorithm is quite robust against the error propagation drawback of successive algorithms. We compare the SER algorithm to the conventional approach in terms of computational complexity and numerical accuracy by simulation, also in the presence of noise.

The paper is outlined as follows: In Sec. II, we review the basics of the NFT and describe how the DT can remove eigenvalues from a nonlinear spectrum. We explain the SER algorithm in Sec. III and explain its robustness against coarse estimation of eigenvalues in Sec. IV. We compare its performance numerically to the conventional approaches in Sec. V. We draw some conclusions in Sec. VI.

II. PRELIMINARIES OF NFT AND DARBOUX TRANSFORM

In a fiber link with ideal distributed amplification, the pulse propagation in a single polarization can be modeled by the nonlinear Schrödinger equation (NLSE),

$$j \frac{\partial q(t, z)}{\partial z} = \frac{\partial^2 q(t, z)}{\partial t^2} + 2 \|q(t, z)\|^2 q(t, z). \quad (1)$$

where t , z and $q(t, z)$ are the normalized time, distance along the fiber and the normalized pulse envelope, respectively. On

a single mode fiber with chromatic dispersion β_2 and Kerr nonlinearity γ , the physical pulse is obtained simply from

$$p(\tau, \ell) = \sqrt{P_0} q \left(\frac{\tau}{T_0}, \ell \frac{|\beta_2|}{2T_0^2} \right), \quad \text{with } P_0 T_0^2 = \frac{|\beta_2|}{\gamma}$$

where T_0 is an arbitrary time-scale, τ and ℓ are the physical time and distance along the fiber.

A. Basics of Nonlinear Fourier Transform

A solution of (1) can be represented in a nonlinear spectrum via the Zakharov Shabat system (ZSS) [10],

$$\frac{\partial}{\partial t} \begin{pmatrix} \vartheta_1(\lambda; t, z) \\ \vartheta_2(\lambda; t, z) \end{pmatrix} = \begin{pmatrix} -j\lambda & q(t, z) \\ -q^*(t, z) & j\lambda \end{pmatrix} \begin{pmatrix} \vartheta_1(\lambda; t, z) \\ \vartheta_2(\lambda; t, z) \end{pmatrix} \quad (2)$$

with the boundary condition

$$\begin{pmatrix} \vartheta_1(\lambda; t, z) \\ \vartheta_2(\lambda; t, z) \end{pmatrix} \rightarrow \begin{pmatrix} 1 \\ 0 \end{pmatrix} \exp(-j\lambda t) \quad \text{for } t \rightarrow -\infty \quad (3)$$

under the vanishing boundary assumption $q(t) \rightarrow 0$ as $t \rightarrow \pm\infty$. The nonlinear (Jost) coefficients are defined as

$$\begin{aligned} a(\lambda; z) &= \lim_{t \rightarrow +\infty} \vartheta_1(\lambda; t, z) \exp(j\lambda t) \\ b(\lambda; z) &= \lim_{t \rightarrow +\infty} \vartheta_2(\lambda; t, z) \exp(-j\lambda t). \end{aligned} \quad (4)$$

The crucial property of the nonlinear spectrum is

$$a(\lambda; z) = a(\lambda; 0), \quad b(\lambda; z) = \exp(-4j\lambda^2 z)b(\lambda; 0). \quad (5)$$

This property indicates that the nonlinear spectrum for each λ evolves independently in z according to this simple equation. This suggests to modulate information on the nonlinear frequencies. We drop the dependency on z , as it is simply multiplicative in (5).

The nonlinear spectrum of $q(t)$ consists of two parts:

- (i) the *discrete spectrum* $\{(\lambda_k, b_k)\}$, where the N eigenvalues $\lambda_k = \omega_k + j\sigma_k \in \mathbb{C}^+$ ($\omega_k, \sigma_k \in \mathbb{R}$) are the roots of $a(\lambda)$ and spectral coefficients $b_k = b(\lambda_k)$.
- (ii) the *continuous spectrum* $Q_c(\lambda) = \frac{b(\lambda)}{a(\lambda)}$ for $\lambda \in \mathbb{R}$.

Note that the discrete spectrum is sometimes defined differently like in [1]. The above representation is chosen as b_k are more preferable for data modulation [11]–[14].

There are various ways to compute the nonlinear spectrum by numerically solving (2) [1], [6], [7], [15], [16]. Practically, it is assumed that the signal $q(t)$ is truncated such that it is non-zero only inside the interval $t \in [T_-, T_+]$. Then the differential equation system (2) can be solved by propagating $\vartheta(\lambda; t)$ from the known solution (3) at the boundary $t = T_-$ to $t = T_+$. The time is discretized with step size h as $t_m = T_- + m \cdot h$ where the sample index is $m = 0, 1, \dots, M-1$.

By applying a change of variables

$$\Psi(\lambda; t) = \begin{pmatrix} \vartheta_1(\lambda; t) \exp(j\lambda t) \\ \vartheta_2(\lambda; t) \exp(-j\lambda t) \end{pmatrix}, \quad (6)$$

one can iterate

$$\mathbf{w}^{(m+1)} = \mathbf{S}_m \mathbf{w}^{(m)} \quad (7)$$

from $\mathbf{w}^{(0)} = \Psi(\lambda; T_-) = (1, 0)^T$ (obtained from the boundary condition (3)) to $\mathbf{w}^{(M)} \approx \Psi(\lambda; T_+)$. Then, according to (4), (6), the spectral coefficients are obtained from

$$\hat{a}(\lambda) = w_1^{(M)}, \quad \hat{b}(\lambda) = w_2^{(M)}. \quad (8)$$

The scattering matrix \mathbf{S}_m depends on the approximation method. Using mid-point approximation, it becomes

$$\mathbf{S}_m = \begin{pmatrix} \cos(|q_m h|) & \frac{q_m \sin(|q_m h|) \exp(2j\lambda t_m)}{|q_m|} \\ -\frac{q_m^* \sin(|q_m h|) \exp(-2j\lambda t_m)}{|q_m|} & \cos(|q_m h|) \end{pmatrix} \quad (9)$$

where q_m are the samples $q(t_m)$ at time t_m . Applying a higher-order approximation method, e.g. [6], [7], results in different \mathbf{S}_m with smaller numerical errors.

The forward-backward method [3] is a modification of the iteration (7). In addition to propagating $\mathbf{w}^{(m)}$ from $t = T_-$ to $t = T_+$, it propagates another vector $\mathbf{u}^{(m)}$ from $t = T_+$ to $t = T_-$ with boundary condition $\mathbf{u}^{(M)} = (0, 1)^T$, i.e.

$$\mathbf{u}^{(m-1)} = \mathbf{S}_m^{-1} \mathbf{u}^{(m)} \quad (10)$$

where \mathbf{S}_m^{-1} is the inverse of \mathbf{S}_m , obtained by changing h to $-h$ in \mathbf{S}_m . Both iterations (7) and (10) are repeated up to some index $0 < p < M$. For $\lambda = \lambda_k$ being an eigenvalue, the estimations of the spectral coefficients are then obtained as

$$\begin{aligned} \hat{a}(\lambda_k) &= w_1^{(p)} u_2^{(p)} - u_1^{(p)} w_2^{(p)} \approx 0 \\ \hat{b}(\lambda_k) &= \frac{w_2^{(p)}}{w_2^{(p)}} \end{aligned} \quad (11)$$

In the next section, we use the following estimate of $\vartheta(\lambda_k; t) = (\vartheta_1(\lambda_k; t), \vartheta_2(\lambda_k; t))^T$. For $m < p$,

$$\hat{\vartheta}(\lambda_k; t_m) \approx \begin{pmatrix} w_1^{(m)} \exp(-j\lambda_k t_m) \\ w_2^{(m)} \exp(j\lambda_k t_m) \end{pmatrix} \quad (12)$$

while for $m > p$

$$\hat{\vartheta}(\lambda_k; t_m) \approx \hat{b}(\lambda_k) \begin{pmatrix} u_1^{(m)} \exp(-j\lambda_k t_m) \\ u_2^{(m)} \exp(j\lambda_k t_m) \end{pmatrix} \quad (13)$$

More accurate estimates are obtained by choosing p according to the criterion in [8].

B. Two Properties of the Darboux Transform

Multi-soliton pulses are specific solutions of the NLSE having only a discrete spectrum. To numerically generate a multi-soliton pulse, an efficient algorithm is based on the DT. It constructs a signal by adding eigenvalues one by one recursively and updating the pulse accordingly. The DT is an elegant approach to modify a pulse by adding a new eigenvalue or also removing an existing one while the rest of the discrete spectrum as well as $b(\lambda)$, $\lambda \in \mathbb{R}$, are unchanged [9]. Let us briefly summarize the DT and its properties. Assume a pulse $q^{(n)}(t)$ with n eigenvalues $\Lambda^{(n)} = \{\lambda_1, \dots, \lambda_n\}$. Consider a complex frequency $\mu \in \mathbb{C}^+$. Let $\vartheta^{(n)}(\mu; t)$ denote a solution of (2) for the pulse $q^{(n)}(t)$. By applying the following transformation,

$$\tilde{q}(t) = q^{(n)}(t) + \frac{2j(\mu^* - \mu)\vartheta_2^{*(n)}(\mu; t)\vartheta_1^{(n)}(\mu; t)}{|\vartheta_1^{(n)}(\mu; t)|^2 + |\vartheta_2^{(n)}(\mu; t)|^2} \quad (14)$$

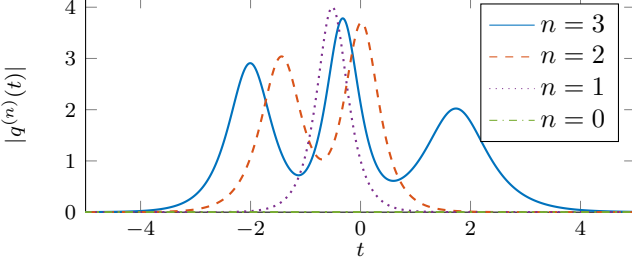


Fig. 1. Example of third order soliton decomposition with initial discrete spectrum $(\lambda_k, b_k) \in \{(1j, 2.1), (1.5j, -0.09), (2j, 0.13)\}$. The dashed pulse is resulted after removal of $\lambda_1 = 1j$ and the dotted pulse is resulted after removal of $\lambda_1 = 1j$ and $\lambda_2 = 1.5j$.

the spectrum of $\tilde{q}(t)$ is related to the one of $q^{(n)}(t)$ according to the following two cases:

1) *Adding Eigenvalues*: If $\mu \notin \Lambda^{(n)}$, then $\tilde{q}(t)$ has $n+1$ eigenvalues $\Lambda^{(n+1)} = \Lambda^{(n)} \cup \{\mu\}$. In this case, we write $\tilde{q}(t) = q^{(n+1)}(t)$. Interestingly, $b(\lambda)$ for $\lambda \in \mathbb{R}$ and b_k for $\lambda_k \in \Lambda^{(n)}$ of $q^{(n+1)}(t)$ stay the same as the ones of $q^{(n)}(t)$ [9]. This property is commonly used to generate a multi-soliton recursively [2], or to generate a pulse with a continuous and discrete spectrum [11].

2) *Removing Eigenvalues*: If $\mu \in \Lambda^{(n)}$, then $\tilde{q}(t)$ has $n-1$ eigenvalues $\Lambda^{(n-1)} = \Lambda^{(n)} \setminus \{\mu\}$. In this case, we write $\tilde{q}(t) = q^{(n-1)}(t)$. Without loss of generality, assume that $\mu = \lambda_n$. Then the relation between the nonlinear spectrum of $q^{(n-1)}(t)$ and the one of $q^{(n)}(t)$ is given by,

$$a^{(n-1)}(\lambda) = \frac{\lambda - \lambda_n^*}{\lambda - \lambda_n} a^{(n)}(\lambda), \text{ for } \lambda \in \mathbb{C} \quad (15)$$

$$\Lambda^{(n-1)} = \{\lambda_1, \dots, \lambda_{n-1}\} \quad (16)$$

$$b^{(n-1)}(\lambda) = b^{(n)}(\lambda), \text{ for } \lambda \in \mathbb{R} \quad (17)$$

$$b_k^{(n-1)} = b_k^{(n)}, \text{ for eigenvalue } \lambda_k, 1 \leq k \leq n-1. \quad (18)$$

Consequently, the remaining eigenvalues and corresponding spectral coefficients do not change if the signal update (14) is applied. In Fig. 1 we show an example of successively applying (14) on a multi-soliton pulse. The pulse has initially 3 eigenvalues which are removed successively in ascending order of their imaginary part. After the last eigenvalue removal, no residual pulse is left.

III. SUCCESSIVE EIGENVALUE REMOVAL ALGORITHM

A. Motivation

Finding the discrete spectrum from (2) is not an easy task. In practice, the tails of a pulse are truncated and then (2) is approximated from the pulse samples. These two steps cause some approximation errors in finding the eigenvalues and spectral amplitudes. A discretized NFT like (7) accumulates the approximation errors. This error is very sensitive to the sampling rate and the truncation. When a pulse has a large support, usually a large sampling rate is required to achieve small errors. A typical observation is that a larger number of eigenvalues in a pulse results in either faster variations of the pulse shape or a longer pulse duration or both. Both effects

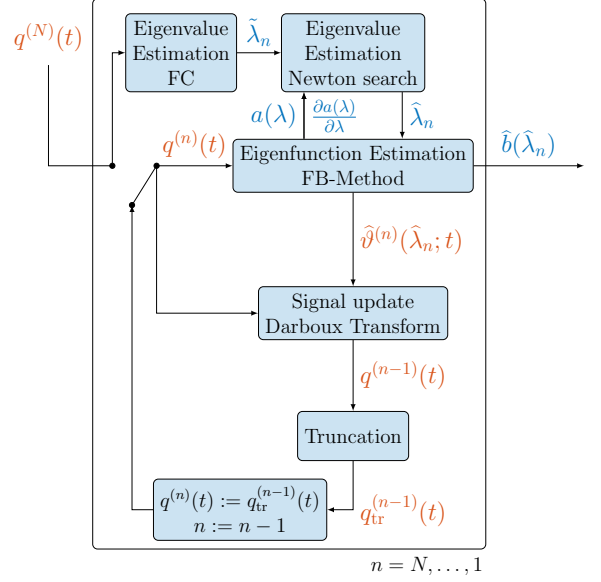


Fig. 2. Block diagram of the Successive Eigenvalue Removal algorithm.

increase the approximation errors. In contrast, removing an eigenvalue may lead to less variations and a reduction in pulse duration. Both effects decrease the number of required samples which leads to a lower computational complexity.

Let us justify the reduction of the pulse duration from the behaviour of the signal tails. Let $q^{(n)}(t)$ denote a multi-soliton pulse with n eigenvalues $\lambda_k = \omega_k + j\sigma_k$, $k = 1, \dots, n$. Assume that the eigenvalues are indexed in decreasing order of their imaginary part, i.e. $\sigma_1 > \sigma_2 > \dots > \sigma_n$. It is shown in [17] that when $t \rightarrow \pm\infty$

$$|q^{(n)}(t)| \sim 4\sigma_n |b_n|^{\pm 1} \exp(\mp 2\sigma_n(t \mp t_s)), \quad (19)$$

$$\text{with } t_s = \frac{1}{2\sigma_n} \ln \left(\left| \prod_{k=1}^{n-1} \frac{\lambda_n - \lambda_k^*}{\lambda_n - \lambda_k} \right| \right). \quad (20)$$

When $|b_k| \sim 1$ for all eigenvalues (i.e. they are in the same order) and eigenvalues are not located too close together (as in practice), removing λ_n (having the smallest imaginary part) decreases t_s and also increases the exponent of (19) resulting in a faster decay in the tails. Both changes can be seen in Fig. 1. Note that removing other eigenvalues reduces also the pulse duration slightly as t_s decreases and the DT enables us to remove eigenvalues in any desired order.

B. Eigenvalue Removal and Truncation

Let $q^{(n)}(t)$ denote a multi-soliton pulse as defined in the previous section. We define the effective pulse support as the smallest time interval $[T_-, T_+]$ such that $|q^{(n)}(t)| \leq 2\sigma_n \sqrt{\varepsilon}$ for $t \notin [T_-, T_+]$ and some small fixed ε . The pulse tails outside $[T_-, T_+]$ are truncated and the pulse duration is then $T = T_+ - T_-$. While other definitions for pulse duration can be taken as well, this definition has the advantage that the truncation threshold scales the same as the pulse energy by normalization of the NLSE (1). For instance, the effective support of a first-order soliton with eigenvalue $j\sigma_n$ contains $\sqrt{1 - \varepsilon}$ fraction of the pulse energy regardless of σ_n value.

As it is shown in Fig. 2, the Successive Eigenvalue Removal (SER) algorithm computes the discrete spectrum of a multi-soliton $q^{(N)}(t)$ in few steps. First, it requires an initial guess of eigenvalues $\hat{\lambda}_k$, $k = 1, \dots, N$ to determine the sequential order of removal and the effective pulse support after each iteration. We use the Fourier collocation (FC) method [18], [19] but one can use any other estimator, e.g. the one finding $\hat{\lambda}_k$ from the continuous spectrum [20]. This step can be skipped when an initial guess of eigenvalues is available. Here, we remove the eigenvalues in the increasing order of their imaginary part as follows:

- (i) [Refinement of eigenvalue] Consider the eigenvalue with smallest imaginary part $\hat{\lambda}_n$. If it is necessary, we improve the eigenvalue estimation further via a Newton zero search $a(\lambda) = 0$ in the neighborhood of $\hat{\lambda}_n$. For that, we estimate $a(\lambda)$ and $\frac{\partial a(\lambda)}{\partial \lambda}$ according to Sec. II-A based on the current pulse $q^{(n)}(t)$. We end up with a more precise eigenvalue estimate $\hat{\lambda}_n$.
- (ii) [Spectral amplitude estimation] We numerically compute the solution $\hat{\vartheta}^{(n)}(\hat{\lambda}_n; t)$ for $t \in [T_-^{(n)}, T_+^{(n)}]$ as described in Sec. II-A. Then, we obtain $\hat{b}(\hat{\lambda}_n)$ from (11).
- (iii) [Eigenvalue removal] We apply the Darboux update (14) to $q^{(n)}(t)$ using $\hat{\vartheta}^{(n)}(\hat{\lambda}_n; t)$ for removing the eigenvalue λ_n (the eigenvalue with smallest imaginary part) from the nonlinear spectrum. The resulting pulse is $q^{(n-1)}(t)$ and has $n-1$ eigenvalues.
- (iv) [Pulse truncation] The pulse support is truncated to the interval $[T_-^{(n-1)}, T_+^{(n-1)}]$ with the truncation threshold of $2\text{Im}\{\hat{\lambda}_{n-1}\}\sqrt{\varepsilon}$.

We repeat these steps until all N eigenvalues are removed.

IV. ANALYSIS OF EIGENVALUE ESTIMATION ERROR

An existing eigenvalue λ_n will be removed by DT from the discrete spectrum, if $\vartheta^{(n)}(\mu; t)$ is computed exactly at $\mu = \lambda_n$. In this section, we explain how the eigenvalue estimation error $\delta = \hat{\lambda}_n - \lambda_n$ affects the capability of the SER algorithm to remove the eigenvalue λ_n . As before, we assume that λ_n is the eigenvalue with the smallest imaginary part.

Since there is always an estimation error $\delta \neq 0$, the SER algorithm indeed adds a new eigenvalue $\hat{\lambda}_n$ to the spectrum. The SER applies the DT signal update (14) at $\mu = \hat{\lambda}_n$ where $\hat{\vartheta}^{(n)}(\mu; t)$ is numerically computed from the pulse $q^{(n)}(t)$. Then, the resulting pulse $\tilde{q}(t)$ has an additional eigenvalue $\hat{\lambda}_n = \lambda_n + \delta$. Note that there are two kinds of error: (i) estimation error δ (ii) numerical errors in $\hat{\vartheta}^{(n)}(\hat{\lambda}_n; t)$. To study only the effect of δ , we use the DT to generate a multi-soliton with discrete spectrum $\{(\lambda_k, b_k)\}_{k=1}^n$ and additionally $\{(\hat{\lambda}_n, \hat{b}_n)\}$ for some arbitrary value \hat{b}_n . When adding $\hat{\lambda}_n$ in the last iteration, one can generate the exact $\vartheta^{(n)}(\hat{\lambda}_n; t)$ as well as $\tilde{q}(t)$. The detailed algorithm is given in [19] and we skip it here.

When $|\delta|$ is small enough, adding $\hat{\lambda}_n$ decomposes $\tilde{q}(t)$ into three separate parts in time domain: two first-order solitons with eigenvalues $\hat{\lambda}_n \approx \lambda_n$ and another pulse between them containing the rest of the discrete spectrum. The separation effect is illustrated in Fig. 3. A multi-soliton with five eigenvalues $\Lambda^{(5)} = \{2.5j, 2j, 1.5j, 1j, 0.5j\}$ (dashed line) is modified

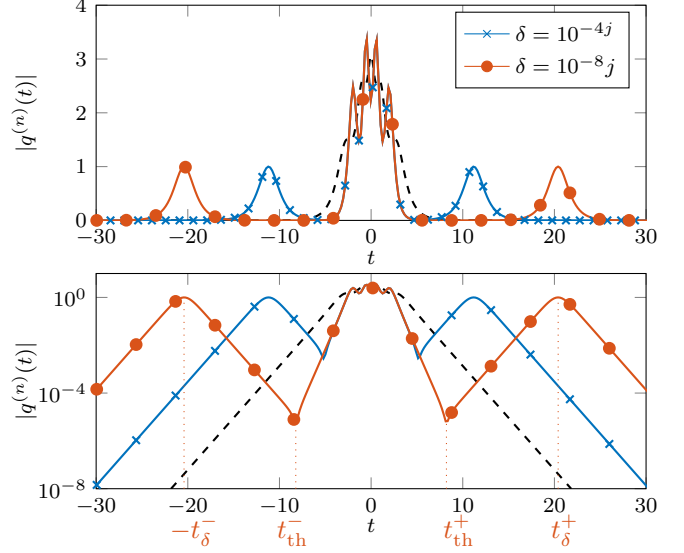


Fig. 3. Addition of $(\hat{\lambda}_n = 0.5j + \delta, \hat{b}_n = \exp(5.88j))$ to a multi-soliton (dashed line) with five eigenvalues $\Lambda^{(5)} = \{2.5j, 2j, 1.5j, 1j, 0.5j\}$, and $b_k = \exp(j\varphi_k)$ of randomly chosen $\varphi_k = 0.24, 4.90, 0.58, 3.98, 0.09$, respectively. The modified pulses $\tilde{q}(t)$ (solid lines) have three parts: two first-order soliton with eigenvalue $\approx 0.5j$ and a multi-soliton with four eigenvalues $\Lambda^{(4)} = \{2.5j, 2j, 1.5j, 1j\}$ in the middle. The distance between two the first-order solitons is $t_\delta^+ + t_\delta^- = O(-\ln(|\delta|))$, given in (22).

by an additional eigenvalue $\hat{\lambda} = 0.5j + \delta$ for two choices of δ . One can observe that the first-order solitons (sech-shape pulses in the tails) are pushed away from the middle part as $|\delta|$ decays. We can analytically approximate the distance between two first-order solitons in terms of δ and spectral amplitude \hat{b}_n . Assume that $|\delta| \ll \sigma_n$ and denote $b_n = |b_n| \exp(j\varphi_n)$ and $\hat{b}_n = |\hat{b}_n| \exp(j\hat{\varphi}_n)$. Similar to the analysis in [17], we write the first-order approximation of the DT update (14) to characterize $\tilde{q}(t)$ when $t \rightarrow \pm\infty$,

$$\tilde{q}(t) \sim -2\sigma_n e^{\mp j\varphi_\delta^\pm - 2\omega_n t} \operatorname{sech}(2\sigma_n(t \mp t_\delta^\pm)) \quad (21)$$

$$\text{with} \quad t_\delta^\pm \approx \frac{1}{2\sigma_n} \ln \left(\left| \frac{2j\sigma_n}{\delta} \prod_{k=1}^{n-1} \frac{\lambda_n - \lambda_k^* \alpha^\pm}{\lambda_n - \lambda_k} \right| \right) \quad (22)$$

$$\varphi_\delta^\pm \approx \arg \left(\frac{2j\sigma_n}{\delta} \prod_{k=1}^{n-1} \frac{\lambda_n - \lambda_k^* \alpha^\pm}{\lambda_n - \lambda_k} \right) \quad (23)$$

$$\alpha^\pm = \left(|\hat{b}_n|^{\pm 1} e^{\pm j\hat{\varphi}_n} - |b_n|^{\pm 1} e^{\pm j\varphi_n} \right) \quad (24)$$

We found in different simulations that the above t_δ^+ and t_δ^- are very close to their numerical values. These values are shown in Fig. 3 for $\delta = 10^{-8}j$.

The distance between two first-order solitons is $t_\delta^+ + t_\delta^- = O(\ln(\frac{1}{|\delta|}))$. Look again at Fig. 3. Let us find the separation points of the three parts of the signal, denoted by t_{th}^\pm . Assume that $|\delta|$ is very small such that the two first-order solitons are far from the middle part. Then, the middle part converges to a multi-soliton with $\{(\lambda_k, b_k)\}_{k=1}^{n-1}$. The separation point t_{th}^+ is approximately equal to the intersection point of the right tail of the middle multi-soliton, given in (19), and the left tail of the first-order soliton on the right, given in (21). Similarly,

we can approximate the separation point t_{th}^- . Accordingly, we obtain

$$t_{\text{th}}^\pm \approx \pm \frac{0.5 \ln \left(|b_{n-1}|^{\pm 1} \frac{\sigma_{n-1}}{\sigma_n} \right) + \sigma_n t_\delta^\pm + \sigma_{n-1} t_0}{\sigma_n + \sigma_{n-1}} \quad (25)$$

$$\text{where } t_0 = \frac{1}{2\sigma_{n-1}} \ln \left(\left| \prod_{k=1}^{n-2} \frac{\lambda_{n-1} - \lambda_k^*}{\lambda_{n-1} - \lambda_k} \right| \right) \quad (26)$$

and $\sigma_{n-1} = \text{Im}\{\lambda_{n-1}\}$.

Now we find a condition on $|\delta|$. After addition of $\hat{\lambda}_n$, the SER algorithm truncates $\tilde{q}(t)$ to the interval $[T_-^{(n-1)}, T_+^{(n-1)}]$. A necessary condition for the truncated signal to contain only the middle part of the signal is $[T_-^{(n-1)}, T_+^{(n-1)}] \subset [t_{\text{th}}^-, t_{\text{th}}^+]$. To satisfy this condition, $|\tilde{q}(t_{\text{th}}^\pm)| < 2\sigma_{n-1}\sqrt{\varepsilon}$. From (19) and (25), we find,

$$\left| \frac{\delta}{\sigma_n} \right| \leq \max \frac{|\alpha^\pm| \sqrt{\varepsilon} \sigma_{n-1}}{\sigma_n} \left(\frac{\sqrt{\varepsilon}}{2|b_{n-1}|^{\pm 1}} \right)^{\frac{\sigma_n}{\sigma_{n-1}}} e^{2\sigma_n(t_s - t_0)} \quad (27)$$

where t_s and t_0 are given in (20) and (26). An interesting advantage of the SER algorithm is that it allows to *detect* whether an eigenvalue has been estimated precisely enough. By removing the eigenvalue λ_n , the pulse energy must decrease by $4\text{Im}(\lambda_n)$. This can be verified by checking the pulse energy after the truncation. Such a capability is missing in other usual NFT algorithms [1], [3]–[5], [15].

V. SIMULATION RESULTS

We compare the SER algorithm to the common NFT methodology that finds all eigenvalues and their spectral coefficients separately without pulse modification. We compare them in terms of computational complexity and estimation accuracy for some exemplary multi-soliton pulses. Note that the absolute accuracy and/or complexity depends on the specific NFT method that is used. However, the SER algorithm can be applied with any underlying NFT method. Thus, although we evaluate all results based on the method in Sec. II-A, the advantage of the SER algorithm is quite general.

A. Pulse Duration and Complexity Reduction

When the ZSS is solved numerically, the computational complexity scales linearly in terms of the pulse samples M . The classical approaches solve the ZSS for all N eigenvalues based on the same given pulse. Although all N eigenvalues can be computed in parallel, the total computational complexity is CNM for some constant C operation cost per sample¹.

The SER algorithm truncates the pulse support after removing each eigenvalue. Recall that $T^{(n)} = T_+^{(n)} - T_-^{(n)}$ is the pulse duration when the pulse has still n eigenvalues. Let $T^{(N)}$ denote the initial pulse duration of a pulse with N eigenvalues. Then the computational complexity is $CM \frac{T^{(n)}}{T^{(N)}}$ if the same NFT algorithm for computing the spectral coefficient of λ_n

¹We assumed the eigenvalues are given. To estimate the eigenvalues by a Newton search, the total complexity is multiplied by the iteration number of the Newton method. We neglect this multiplication factor for simplicity as it is almost the same for the SER algorithm and the other methods.

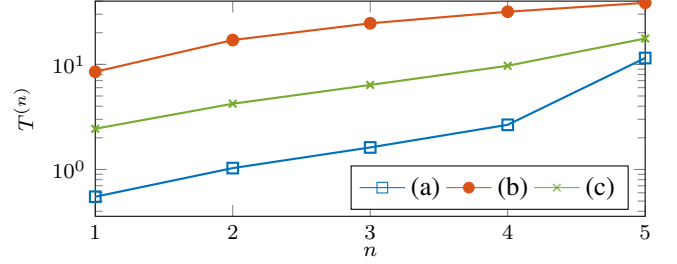


Fig. 4. Pulse duration $T^{(n)}$ for n remaining eigenvalues after each iteration of the SER algorithm. Three multi-soliton pulses are considered with (a) $\Lambda_a^{(5)} = \{9j; 7j; 5j; 3j; 0.5j\}$, (b) $\Lambda_b^{(5)} = \{0.58j; 0.56j; 0.54j; 0.52j; 0.5j\}$ and (c) $\Lambda_c^{(5)} = \{2.5j; 2j; 1.5j; 1j; 0.5j\}$.

is applied. The total complexity of the SER algorithm is then $\alpha_N CNM$ with $\alpha_N = \frac{\sum_{n=1}^N T^{(n)}}{NT^{(N)}}$.

The SER algorithm has a factor α_N smaller complexity than a classical approach. The complexity gain, however, depends on the nonlinear spectrum of the pulse. Fig. 4 shows how the pulse duration $T^{(n)}$ decreases after each SER iteration for three exemplary multi-solitons with 5 eigenvalues. Three sets of eigenvalues are chosen: (a) $\Lambda_a^{(5)} = \{9j; 7j; 5j; 3j; 0.5j\}$, (b) $\Lambda_b^{(5)} = \{0.58j; 0.56j; 0.54j; 0.52j; 0.5j\}$, and (c) $\Lambda_c^{(5)} = \{2.5j; 2j; 1.5j; 1j; 0.5j\}$. For all three pulses, we let $b_k = (-1)^k$ and $\varepsilon = 2 \cdot 10^{-4}$. For the chosen soliton examples, the complexity reduces by α_N (a) ≈ 0.3 , (b) ≈ 0.62 and (c) ≈ 0.46 , respectively. Note that from (19), the pulse duration $T^{(n)}$ can be well approximated as

$$T^{(n)} \approx 2t_s + \frac{1}{2\sigma_n} \ln \left(\frac{4}{\varepsilon} \right) \quad (28)$$

for sufficiently small ε . We see that, up to the first-order approximation, $T^{(n)}$ is independent of the spectral phases φ_k .

The FC method was not considered in the complexity analysis as its complexity is independent of the SER algorithm. Note, however, that the FC can provide a coarse eigenvalue estimate with only a few samples [19]. If predefined eigenvalues are used for modulation, FC is not needed at all.

B. Estimation Accuracy

We compare the precision of the SER algorithm and the common NFT methodology in finding the spectral coefficients of a given pulse. To have a fair comparison, the SER algorithm should use the same NFT algorithm to find $\hat{\vartheta}^{(n)}(\hat{\lambda}_n; t)$. Here, we use the NFT algorithm of Sec. II-A. We consider the eigenvalue set $\Lambda_c^{(5)}$ with $b_k = \exp(j\varphi_k)$. We generate 5000 multi-soliton pulses $q^{(5)}(t)$ with randomly chosen φ_k values. Let us define the bandwidth B of a pulse in (linear) Fourier domain as the frequency support containing 99.99% of the total energy. All pulses are sampled with the same sampling rate of $f_s = 4 \max_{\varphi_k} B$. We further add a white Gaussian noise to the pulses according to a signal-to-noise ratio (SNR) defined within the bandwidth B_{max} . Then, we compute the spectral coefficients $\hat{b}(\hat{\lambda}_k)$ of the noisy pulses using both algorithms. Define $\hat{\varphi}_k = \arg\{\hat{b}(\hat{\lambda}_k)\}$. Fig. 5 shows the variance of the phase error, $\text{Var}(\hat{\varphi}_k - \varphi_k)$, in terms of

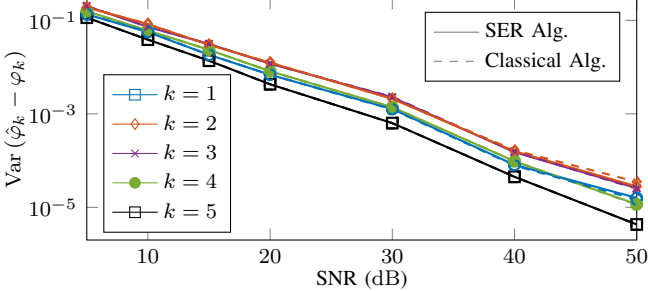


Fig. 5. Accuracy of the SER algorithm in comparison to the classical NFT algorithm of Sec. II-A for the detection of the spectral amplitudes $b(\lambda_k) = \exp(j\phi_k)$. The variance of the phase estimation error $\text{Var}(\hat{\varphi}_k - \varphi_k)$ in terms of SNR for a multi-soliton pulse with $\Lambda_c^{(5)} = \{2.5j; 2j; 1.5j; 1j; 0.5j\}$ being perturbed by an additive white Gaussian noise is shown.

SNR for both algorithms. We observe that both algorithms have quite the same precision while the SER algorithm has about half the complexity.

The SER algorithm reduces the complexity by pulse truncation. We now compare the performance of the SER and the classical algorithm when both algorithms have the same total number of samples (and thus the same complexity). One interesting scenario is to investigate how the performance of the classical NFT algorithm is sensitive to the pulse truncation. The logic behind this scenario is to see how the contribution of an eigenvalue is distributed over the support of an initial pulse. We choose the pulse truncations according to the SER algorithm: $T^{(5)}, T^{(4)}, T^{(3)}, T^{(2)}, T^{(1)}$ as given in Fig. 4. The pulses are generated and sampled as explained before at SNR = 30dB. We compute the spectral coefficients using the classical NFT methodology when applying the different truncations $T^{(n)}$. Fig. 6 shows the respective $\text{Var}(\hat{\varphi}_k - \varphi_k)$ for all eigenvalues with different truncation. The dashed line indicates the performance of the SER algorithm. The dotted line is the performance of the classical NFT algorithm when it applies the same truncation value $T^{(n)}$ as in the SER algorithm before finding each $\hat{b}(\hat{\lambda}_n)$. This way, it uses the same number of samples as the SER algorithm but its performance degrades significantly. In fact, any pulse truncation causes a drastic growth in the estimation error without applying the SER pulse modification. On the other hand, by applying the pulse modification of SER algorithm, the nonlinear spectral contents will be condensed in a shorter time support.

VI. CONCLUSION

We proposed the successive eigenvalue removal algorithm to compute the discrete spectrum. The algorithm computes the spectral coefficients successively and carefully removes the previously computed eigenvalue and its spectral coefficient from the spectrum. The algorithm peels off the eigenvalues of a pulse one by one to simplify the computation of the remaining discrete spectrum. As an application, we showed a considerable complexity gain of the SER algorithm compared to the conventional methodology without pulse modification in finding the spectral coefficients without sacrificing accuracy.

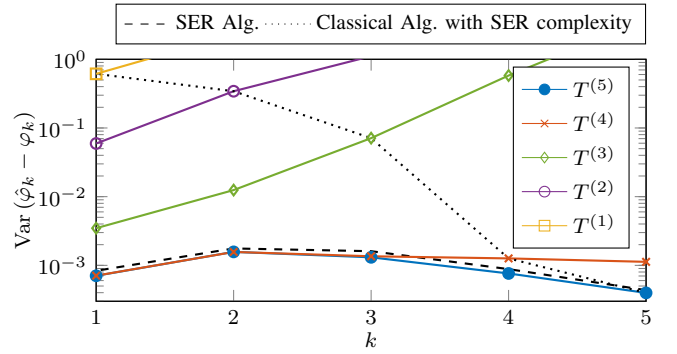


Fig. 6. Effect of a pulse truncation $T^{(n)}$ on the accuracy of a classical NFT algorithm to detect $b(\lambda_k) = \exp(j\phi_k)$. The variance of the phase estimation error $\text{Var}(\hat{\varphi}_k - \varphi_k)$ is shown for a randomly phase modulated multi-soliton pulse with $\Lambda_c^{(5)} = \{2.5j; 2j; 1.5j; 1j; 0.5j\}$ with an additive white Gaussian noise perturbation at SNR = 30dB. The dashed line shows the result when using the SER algorithm. The dotted line is the accuracy of the classical NFT algorithm when applying the same truncation value $T^{(n)}$ as in the SER algorithm before finding the respective $\hat{b}(\hat{\lambda}_n)$.

REFERENCES

- [1] M. I. Yousefi and F. R. Kschischang, "Information transmission using the nonlinear fourier transform, part i-iii," *IEEE Trans. Inf. Theory*, vol. 60, no. 7, 2014.
- [2] V. B. Matveev and M. A. Salle, *Darboux transformations and solitons*. Springer-Verlag, 1991.
- [3] V. Aref, "Control and detection of discrete spectral amplitudes in nonlinear fourier spectrum," *arXiv preprint arXiv:1605.06328*, 2016.
- [4] S. Hari and F. Kschischang, "Bi-directional algorithm for computing discrete spectral amplitudes in the nft," *Journal of Lightwave Technology*, vol. 34, no. 15, pp. 3529–3537, 2016.
- [5] A. Vasylchenko, J. E. Prilepsky, D. Shepelsky, and A. Chattopadhyay, "Direct nonlinear fourier transform algorithms for the computation of solitonic spectra in focusing nonlinear schrödinger equation," *Communications in Nonlinear Science and Numerical Simulation*, vol. 68, pp. 347–371, 2019.
- [6] S. Chimalgali, P. J. Prins, and S. Wahls, "Fast nonlinear fourier transform algorithms using high order exponential integrators," in *Signal Processing in Photonic Communications*, 2018.
- [7] S. Medvedev, I. Vaseva, I. Chekhovskoy, and M. Fedoruk, "Exponential fourth order schemes for direct zakharov-shabat problem," *Opt. Express*, vol. 28, no. 1, pp. 20–39, Jan 2020.
- [8] P. J. Prins and S. Wahls, "Soliton phase shift calculation for the korteweg-de vries equation," *IEEE Access*, vol. 7, 2019.
- [9] L. Junmin, "Evolution of the scattering data under the classical darboux transform for $su(2)$ soliton systems," *Acta Mathematicae Applicatae Sinica*, vol. 6, no. 4, 1990.
- [10] A. Shabat and V. Zakharov, "Exact theory of two-dimensional self-focusing and one-dimensional self-modulation of waves in nonlinear media," *Soviet physics JETP*, vol. 34, no. 1, p. 62, 1972.
- [11] V. Aref, S. T. Le, and H. Buelow, "Modulation over nonlinear fourier spectrum: Continuous and discrete spectrum," *Journal of Lightwave Technology*, 2018.
- [12] T. Gui, T. H. Chan, C. Lu, A. P. T. Lau, and P.-K. A. Wai, "Alternative decoding methods for optical communications based on nonlinear fourier transform," *Journal of Lightwave Technology*, vol. 35, no. 9, May 2017.
- [13] H. Buelow, V. Aref, and L. Schmalen, "Modulation on discrete nonlinear spectrum: Perturbation sensitivity and achievable rates," *IEEE Photonics Technology Letters*, 2018.
- [14] X. Yangzhang, V. Aref, S. T. Le, H. Buelow, D. Lavery, and P. Bayvel, "Dual-polarization non-linear frequency-division multiplexed transmission with b -modulation," *Journal of Lightwave Technology*, vol. 37, no. 6, pp. 1570–1578, 2019.
- [15] S. Wahls and H. V. Poor, "Fast numerical nonlinear fourier transforms," *IEEE Trans. Inf. Theory*, vol. 61, no. 12, pp. 6957–6974, 2015.
- [16] S. K. Turitsyn, J. E. Prilepsky, S. T. Le, S. Wahls, L. L. Frumin, M. Kamalian, and S. A. Derevyanko, "Nonlinear fourier transform for optical data processing and transmission: advances and perspectives," *Optica*, vol. 4, no. 3, March 2017.

- [17] A. Span, V. Aref, H. Bülow, and S. ten Brink, "Time-bandwidth product perspective for nonlinear fourier transform based multi-eigenvalue soliton transmission," *IEEE Transactions on Communications*, 2019.
- [18] J. Yang, *Nonlinear waves in integrable and nonintegrable systems*. Siam, 2010, vol. 16.
- [19] F. J. García-Gómez and V. Aref, "Statistics of the nonlinear discrete spectrum of a noisy pulse," *Journal of Lightwave Technology*, 2019.
- [20] V. Aref, S. T. Le, and H. Buelow, "An efficient nonlinear fourier transform algorithm for detection of eigenvalues from continuous spectrum," in *Optical Fiber Communication Conference*. Optical Society of America, 2019, pp. M1I-5.